ACS APPLIED MATERIALS & INTERFACES

Research Article

www.acsami.org

# Proton Exchange Membrane Developed from Novel Blends of Polybenzimidazole and Poly(vinyl-1,2,4-triazole)

Mousumi Hazarika and Tushar Jana*

School of Chemistry, University of Hyderabad, Hyderabad, India

Supporting Information

**ABSTRACT:** In continuation (*J. Phys. Chem. B* **2008**, *112*, 5305; *J. Colloid Interface Sci.* **2010**, *351*, 374) of our quest for proton exchange membrane (PEM) developed from polybenzimidazole (PBI) blends, novel polymer blend membranes of PBI and poly(1-vinyl-1,2,4-triazole) (PVT) were prepared using a solution blending method. The aim of the work was to investigate the effect of the blend composition on the properties, e.g., thermo-mechanical stability, swelling, and proton conductivity of the blend membranes. The presence of specific interactions between the two polymers in the blends were observed by studying the samples using varieties of spectroscopic techniques. Blends prepared in all possible compositions were studied using a differential scanning calorimetry (DSC) and exhibited a single $T_g$ value, which lies between the $T_g$ value of the neat polymers. The presence of a single composition-dependent $T_g$ value indicated that the blend is a miscible blend. The N−H···N interactions between the two polymers were found to be the driving force for the miscibility. Thermal stability up to 300 °C of the blend membranes, obtained from thermogravimetric analysis, ensured their suitability as PEMs for high-temperature fuel cells. The proton conductivity of the blend membranes have improved significantly, compared to neat PBI, because of the presence of triazole moiety, which acts as a proton facilitator in the conduction process. The blend membranes showed a considerably lower increase in thickness and swelling ratio than that of PBI after doping with phosphoric acid (PA). We found that the porous morphology of the blend membranes caused the loading of a larger amount of PA and, consequently, higher proton conduction with lower activation energy, compared to neat PBI.

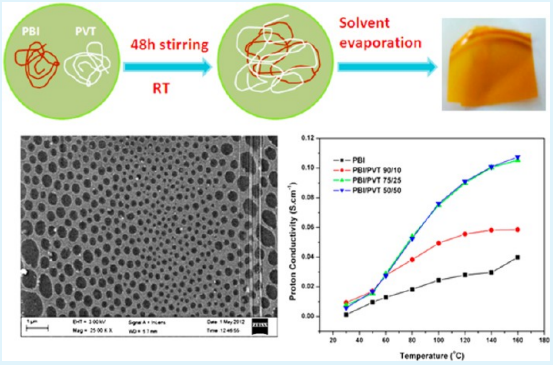


**KEYWORDS:** *proton exchange membranes, polybenzimidazole, poly (1-vinyl-1,2,4-triazole), miscible blend, proton conductivity*

## INTRODUCTION

Proton exchange membrane fuel cells (PEMFCs) have received significant attention as promising candidates for clean and efficient energy conversion devices.[1−3] The conventional perfluorinated polymer-based proton exchange membrane (PEM) can operate only at low temperature; above 120 °C, this PEM displays negligible proton conductivity. Therefore, the last couple of years, an enormous amount of effort has been exerted to develop high-temperature PEMs that can conduct protons readily up to 180 °C.[4−12] Fuel cells consisting of this type of PEM offers many advantages, including simpler water management, higher CO tolerance, and faster electrode kinetics.[8−14] Heteroaromatic polymers containing groups such as imidazole, pyrazole, and triazole exhibit high conductivity in the anhydrous state at higher temperature and they are found to be suitable for fabricating high-temperature PEMs.[15−19] The basic nitrogen sites of these heterocyclic polymers act as strong proton acceptors, with respect to strong acid groups, and thus facilitate the proton conduction when doped with acid at higher temperature.[20,21]

Triazole and its derivatives have been studied extensively for use in high-temperature PEMs because of their excellent proton conduction behavior.[22−29] 1H-1,2,4-triazole, a heterocyclic molecule, can conduct protons readily under anhydrous conditions at higher temperature (>100 °C) via the Grotthuss mechanism as in imidazole. The reported proton conductivity of pure 1H-1,2,4-triazole is $1.5 \times 10^{-4}$ S/cm (at 115 °C) and $\sim 1.2 \times 10^{-3}$ S/cm (at the melting point).[22] Three N atoms in the triazole ring increase the long-range proton transport via structure diffusion, which is the driving force for the proton conduction. In several reports, 1H-1,2,4-triazole has been used as a dopant in an acidic polymer or to modify a polymer backbone with triazole units.[22,30−32] The disadvantage of using triazole as a dopant is that it may form a liquid phase in the polymer matrix, because of its low melting point, which results in diffusion from the polymer matrix into the electrodes and, at high humidity, because of its solubility, triazole may go out of the membrane.[26]

Poly(1-vinyl-1,2,4-triazole) (PVT, Scheme 1) is an promising polymer where the triazole ring is attached to the polymer backbone and, hence, can be used as an PEM in high-temperature fuel cells after doping with appropriate dopants.

**Received:** July 2, 2012
**Accepted:** September 6, 2012
**Published:** September 6, 2012

**Scheme 1. Structure of (A) Poly[2,2′-(*m*-phenylene)-5,5′-benzimidazole] (PBI) and (B) Poly(1-vinyl-1,2,4-triazole) (PVT)**

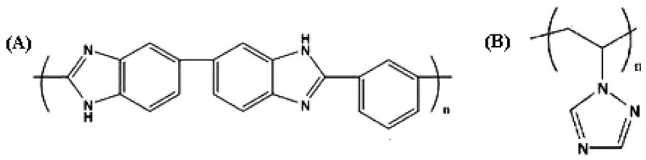


Bozkurt et al.[33−35] has pioneered the PVT-doped membranes for their use as PEMs. They doped the polymer with a variety of acids at various molar ratios and showed that proton conductivity increases with dopant concentration and temperature. The mechanism of proton conductivity in the membranes was found to be the Grotthuss mechanism. The proton conductivity increased as the amount of dopant concentration, as well as the temperature, increased. But the main drawback of this polymer is that it does not form films that are very strong mechanically and, hence, its use may be limited.

Polymer blending is an easy and economical method to produce new polymeric materials, because, by mixing two or more polymers with different physical properties, a material with enhanced physical and chemical properties can be generated. Therefore, the blending of PVT with another polymer, which can provide mechanical strength without destroying the other properties (such as proton conducting character) can be useful for the development of free-standing mechanically strong films with high thermal stability and high proton conductivity. The reported Nafion/PVT blend[36] membranes were homogeneous and thermally stable at least up to 300 °C and have displayed a conductivity that increased by three orders of magnitude upon hydration. But this blend membrane cannot be used for high-temperature proton exchange membranes (HT-PEMs). Hence, the search for another polymer that can be blended with PVT is still ongoing for the development of HT-PEM.

Phosphoric acid (PA)-doped polybenzimidazole (PBI, Scheme 1) has received much attention over the past few years and, to date, it is the best-known alternative of Nafion for high-temperature operations. PA-doped PBI exhibits high proton conductivity at temperatures up to 200 °C and very high mechanical stability. It has some other advantages also, such as low gas permeability, excellent oxidative and thermal stability, and an almost-zero water drag coefficient. The proton conductivity of PA-doped PBI membranes is dependent on the doping level. PBI possesses both proton donor (−NH−) and proton acceptor (−N═) hydrogen bonding sites. Because of the availability of the hydrogen bonding sites in the polymer backbone, it can form miscible blends[37,38] with a variety of polymers. So the blend of PVT with PBI would be interesting, because combining the two polymers may result in a material where the properties of both polymers will combine and, as a result, the material may show high proton conductivity with high thermal and mechanical stability. We have demonstrated, in a series of articles, that PBI forms miscible and partially miscible blends with a variety of polymers, such as poly(vinylidene fluoride), sulfonated polystyrene, and poly(vinylidene fluoride-co-hexafluoropropene).[39,40] In all of these cases, we have observed that, upon blending, the PBI properties (especially proton conduction behavior) have improved significantly. Therefore, we expect to see better conduction properties in the current blend also.

In the present work, PVT, which has also acceptor sites in the side chain, was synthesized by free radical polymerization and blended with PBI. The miscibility, thermal stability, and proton conductivity of the blend membranes are studied using a variety of spectroscopic, thermal, and electrical techniques, respectively. Morphology of blend membranes was probed by microscopic techniques to understand the micro structural influences on the properties.

## EXPERIMENTAL SECTION

**Materials.** Poly [2,2′-(*m*-phenylene)-5,5′-benzimidazole] (PBI) was obtained by polymerizing 3,3′,4,4′-tetraaminobiphenyl (TAB) and isophthalic acid in a polyphosphoric acid medium (115%) in the laboratory, using the standard method that we described earlier.[41,42] The measured inherent viscosity (IV) from $H_2SO_4$ solution is 1.04 dL/g and the calculated viscosity-average molecular weight is 70 000. The concentration of the polymer solution in $H_2SO_4$ was 0.2 g/dL for the viscosity measurements. The viscosity-average molecular weights of the PBI samples were obtained using the Mark−Houwink equation, where $K = 5.2 \times 10^{-5}$ dL/g and $a = 0.92$ for $H_2SO_4$ (98%) solvent at 30 °C. The intrinsic viscosity ($[\eta]$) values of the synthesized PBIs were obtained using the Kuwahra single-point method. 1-Vinyl-1,2,4-triazole (>97%) was purchased from Sigma−Aldrich. Azobisisobutyronitrile (AIBN) is recrystallized from tetrahydrofuran (THF). Dimethylacetamide (DMAc; HPLC grade), dimethyl formamide (DMF; HPLC grade), phosphoric acid PA (85%), and deuterated dimethyl sulfoxide (DMSO-$d_6$) were obtained from Merck (India) and used as-received.

**Synthesis of Poly(1-vinyl-1,2,4-triazole).** Poly(1-vinyl-1,2,4-triazole) (PVT) was synthesized via a free-radical polymerization method, using AIBN (5 mol %) as an initiator.[43] The monomer weight concentration is 10%, with respect to DMF as solvent. The reaction mixture was heated at 60 °C under a $N_2$ environment for 24 h. After polymerization, the solution was poured into a large excess of ether. The resulting precipitate was washed in ether and dried in a vacuum oven at 60 °C for 1 day. The IV value of the polymer measured from DMSO solution is 2.69 dL/g, and the calculated viscosity-average molecular weight using the Mark−Houwink equation is 12 000. The PVT polymer was confirmed using $^{13}C$ CP-MAS NMR (SS-NMR) and FT-IR spectroscopy (see Figures 1 and 2 in the Supporting Information). The NMR spectrum of PVT consists of four lines. The peaks near 150 and 158 ppm are the characteristic C peaks of the triazole ring, and the peaks near 45 and 58 ppm correspond to the A and B peaks of the polymer backbone.[33−35] The FT-IR spectrum of PVT contains the characteristic peaks of N═N, C═N, and C−N stretching frequencies at 1277, 1434, and 1659 $cm^{-1}$, respectively. The peak at 3438 $cm^{-1}$ is due to absorbed moisture.

**Blend Preparation.** Blends were prepared by mixing two polymers (PBI and PVT) in DMAc. The concentration of the polymer solution in DMAc was kept 1% (w/v). The required amount of the two polymers was taken in the measured quantity of DMAc and mixing was continued for 2 days by stirring with the help of a magnetic stirrer in a closed glass vessel at room temperature. The homogeneous blend solutions were filtered through a 0.2-$\mu$m polytetrafluoroethylene (PTFE) membrane and then poured into a clean glass Petri dish at 70 °C to cast the blend films. Transparent homogeneous thin films (see Figure 3 in the Supporting Information) were obtained and dried in a vacuum oven at 70 °C for 3 days to evaporate the trace amount of solvent completely. The films were stored in a closed desiccator for further characterization.

**Characterization Techniques.** *FT-IR and NMR Spectroscopy.* Fourier transform infrared (FT-IR) spectra of the thin blend films (~70 $\mu$m) were recorded on Nicolet 5700 FT-IR spectrometer at a resolution of 0.5 $cm^{-1}$ with an average of 64 scans. $^{13}C$ CP-MAS measurements were performed using a Bruker 400 MHz NMR spectrometer.

*Absorption and Fluorescence Spectroscopy.* Electronic absorption spectra were recorded on a Shimadzu model UV-3100 UV−visible spectrometer. Steady-state fluorescence emission spectra were recorded on a Jobin−Yvon Horiba spectrofluorimeter (Model Fluoromax-3). The 1% PBI and blend solutions in DMAc were spin-coated onto an optically transparent quartz plate, and then the spectra were recorded from the spin-coated plate.

*Thermal Study.* Thermogravimetric and differential thermal analysis (TG-DTA) were carried out on a Netzsch STA 409PC TG-DTA instrument, from 50 °C to 800 °C, with a scanning rate of 10 °C/min in the presence of a nitrogen flow. A differential scanning calorimetry (DSC) device (Pyris Diamond DSC, Perkin−Elmer) was used to study the glass-transition temperatures ($T_g$) of the blend samples. Samples were kept at 50 °C for 30 min under isothermal conditions. Samples then were scanned from 50 °C to 450 °C at a heating rate of 10 °C/min. The PVT and blend samples with high PVT content (10/90) were scanned up to temperatures of 200 °C. The reproducibility of DSC results was checked by repeating the experiment at least thrice. The DSC equipment was calibrated using In and Zn as calibration materials prior to scanning the blend samples.

*Morphological Investigations.* The morphology of the blend samples were studied using field-emission scanning electron microscopy (FESEM). The samples were prepared by depositing one drop of 1% solution of the neat polymers and the blend samples on a glass slide. The glass slides then were dried in an oven at 60 °C. They then were coated with gold, and their micrographs were obtained using a FESEM apparatus (Model Ultra 55, Carl Zeiss)

*Doping Level, Swelling Ratio and Thickness Increase after Doping with Phosphoric Acid.* The phosphoric acid doping level was calculated as the number of moles of PA present per PBI repeat unit. Doping level, swelling ratio, and thickness increase measurements were carried out by immersing the dry membranes in phosphoric acid (PA) for 3 days. The weight ($W_d$), length ($L_d$), and thickness ($T_d$) of the membrane were measured before dipping in PA. The weight ($W_w$), length ($L_w$) and thickness ($T_w$) of the wet membranes were measured after 3 days of dipping in PA. Surface-absorbed PA was wiped before the measurements. Swelling ratio and thickness increase values of the membranes were calculated as

$$\text{swelling ratio (\%)} = \frac{L_w - L_d}{L_d} \times 100 \quad (1)$$

$$\text{thickness increase (\%)} = \frac{T_w - T_d}{T_d} \times 100 \quad (2)$$

The doping level calculation was determined by finding the weight of the acid absorbed by the membranes and for that the doped membranes that were dried in a vacuum oven at 100 °C for 24 h and then weighed ($W_{acid}$). Equation 3 was used to calculate the number of moles of PA per PBI repeat unit.

$$\text{Doping level (mols PA/PBI repeat unit)} = \frac{W_{acid} - W_d}{W_d \times F_{PBI}} \times \frac{MW_{PBI}}{MW_{PA}} \quad (3)$$

where $MW_{PA}$ and $MW_{PBI}$ are the molecular weights of PA and PBI, respectively. $F_{PBI}$ is the weight fraction of PBI in the blend compositions. All of the measurements were carried out with three different pieces of similarly sized samples. The results represented here are the averages of three sets of data.

*Conductivity Study.* A four-point-probe technique is used to measure the proton conductivities of the blend samples. The impedance of the membranes were measured with an impedance analyzer, using a Zahner impedance spectrometer (ZENNIUM PP211) over a frequency range from 1 Hz to 100 Hz. The acid-loaded membrane was cut into a rectangular shape and mounted onto the in-house-built conductivity cell. First, the conductivity of the membranes was measured from 30 °C to 160 °C. After the first heating scan, the cell is cooled while maintaining the dry conditions inside the vacuum and, again, the conductivity was measured from 30 °C to 160 °C. The data presented here are the second heating scan data. The conductivities of the samples were obtained from the direct-current potential difference between the two inner electrodes. The conductivity was calculated with the following equation:

$$\sigma = \frac{D}{RBL} \quad (4)$$

where $\sigma$ is the proton conductivity (S/cm), $D$ is the distance between the electrodes, and $B$ and $L$ are the thickness and width of the blend samples, respectively. In all cases, $R$ was obtained from the Nyquist plots.

## RESULTS AND DISCUSSION

**FT-IR Study.** The FT-IR spectra of PBI, PVT, and blend samples (collected from thin films) in the 3600−3000 $cm^{-1}$ region are shown in Figure 1. Spectra of PBI consists several

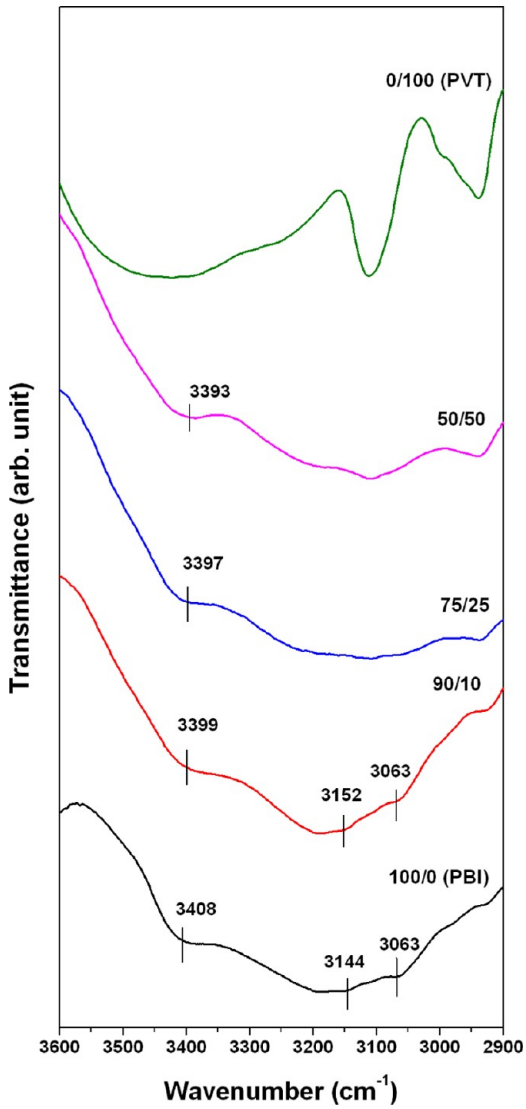


**Figure 1.** FT-IR spectra (3600−2900 $cm^{-1}$) of the PBI/PVT blend film samples at their indicated compositions.

N−H stretching bands in the 3600−3000 $cm^{-1}$ region. The peak at 3408 and 3144 $cm^{-1}$ are because of free non-hydrogen-bonded N−H stretching and self-associated N−H stretching, respectively.[37−40] The peak at 3063 $cm^{-1}$ is due to the stretching frequency of aromatic C−H groups. It is observed that the peak at 3408 $cm^{-1}$ is shifting to lower frequency and

becomes broad with increasing PVT concentration (Figure 1). In case of the 50/50 blend, the peak shifted to 3393 $cm^{-1}$. This peak is not visible in 25/75 and 10/90 (PBI/PVT) blends, because of overlapping of the PVT peaks with these peaks. However, the aromatic stretching peak at 3063 $cm^{-1}$ does not change its position. The red-shift of the free N−H band upon blending indicates the formation of specific interactions between N−H groups of PBI with functionalities of PVT. From Figure 1, it is also observed that the self-associate N−H peak at 3144 $cm^{-1}$ is shifting toward higher frequency and increases its intensity. In the case of the 90/10 blend, the peak shifted to 3152 $cm^{-1}$. This shifting and intensity enhancement can be attributed to the weakening of self-associated N−H−N hydrogen bonding of the PBI chains. Hence, from the IR studies, it is clearly evident that the N−H functionalities of PBI take part in the interaction with PVT upon blending.

It is expected that the interaction between the two polymers will also induce changes in the PVT stretching frequencies. To understand this, we carefully analyze the FT-IR spectra of PVT, PBI, and blend films in the region of 1700−1150 $cm^{-1}$ (Figure 2). The peak at 1277 $cm^{-1}$ in pure PVT represents the characteristic peak of the ring N−N bond. The peak at 1434 and 1659 $cm^{-1}$ are the characteristic peaks of C−N and C═N bonds, respectively.[33−35] Among three N atoms of the PVT ring, one is connected to the vinyl chain; hence, it cannot be involved in any interaction. The other two N atoms can form hydrogen bonding with N−H group of PBI. From Figure 2, it is visible that the N−N stretching frequency at 1277 $cm^{-1}$ is broadened and shifts to higher frequency as the PBI content in the blend is increased. When the PBI content is 90%, the 1277 $cm^{-1}$ peak is shifted to 1285 $cm^{-1}$. The peak at 1434 $cm^{-1}$ does not change its position but becomes broad with increasing PBI content in the blend. As the PBI content in the blend is increased, the peak at 1659 $cm^{-1}$ is shifted to lower frequency and shows substantial broadening. These changes indicated that a N−H···N type of interaction is present between the two polymers. Thus, IR data confirmed the presence of hydrogen-bond interactions between the two polymers in the blend.

**Solid State $^{13}$C CP-MAS study.** The interactions of the blend components can induce changes in line shape and/or shifts in the $^{13}$C resonance frequencies in the NMR spectra of the blend components, in comparison with the spectra of the neat polymers. Solid-state NMR has been used to study the interactions in the blends, because of the fact that this type of interaction strongly influences the electron density around the carbons bearing the interacting functionalities and induce changes in carbon chemical shifts, as well as changes in line shape. The solid-state NMR spectra of the PBI, PVT, and blend samples are shown in Figure 3. The spectrum of PBI consists of several lines. The peak at 155 ppm is due to the carbons of the imidazole rings attached to phenylene rings, the peak at 146

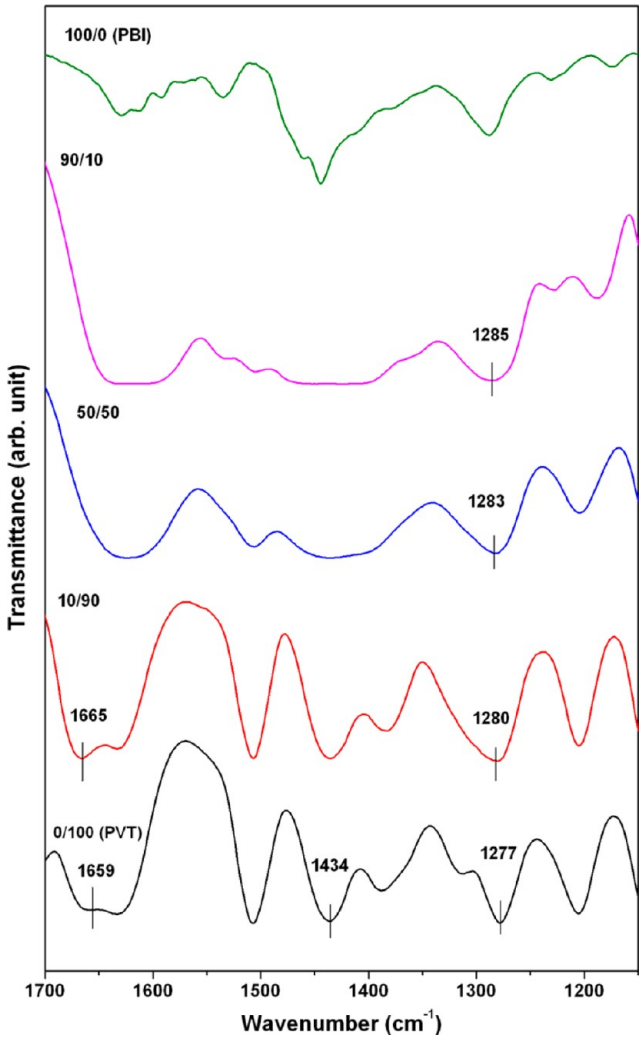


Figure 2. FT-IR spectra (1700−1100 $cm^{-1}$) of the PBI/PVT blend film samples at their indicated compositions.

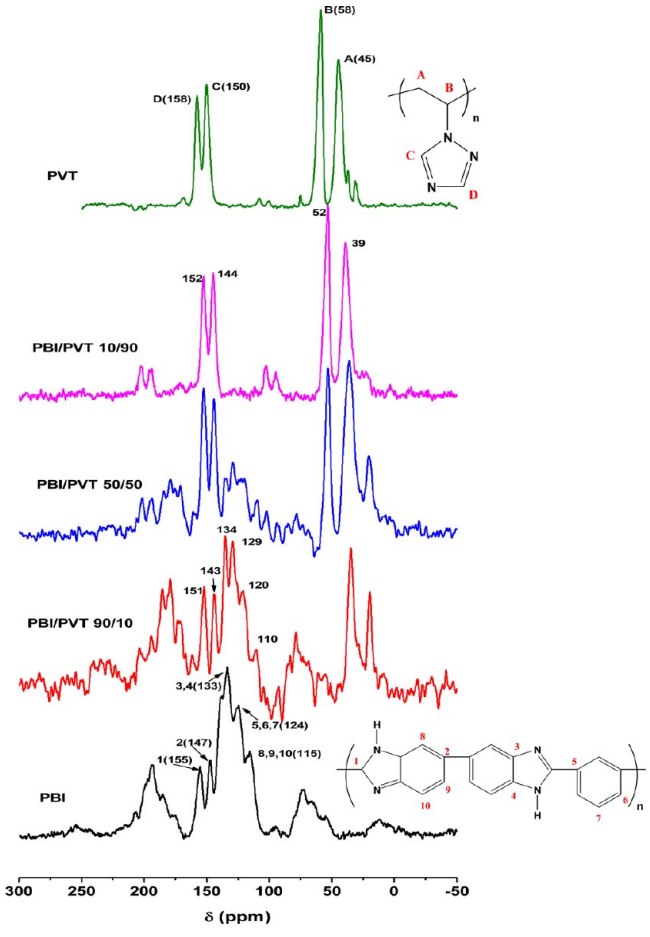


Figure 3. $^{13}$C CPMAS NMR spectra of PBI, PVT, and blend samples.


dx.doi.org/10.1021/am301185b | ACS Appl. Mater. Interfaces 2012, 4, 5256−5265

ppm is due to the carbons that connect the benzimidazole rings in the benzimidazole system, and the peak at 133 ppm is due to the aromatic carbons bound to the N atoms. The remaining peaks at 124 and 115 ppm are due to the protonated carbons of PBI with a contribution from the nonprotonated carbon of the phenylene ring to the line centered at 124 ppm.[44] The PVT spectra consist of four lines. The peaks near 150 and 158 ppm are the characteristic C and D peaks of the triazole ring, and the peak near 45 and 58 ppm corresponds to structures A and B of the polymer backbone. From Figure 3, it is observed that the PBI peaks 155, 147, 133, 124, and 115 ppm have been shifted to the higher field in the case of the PBI/PVT blends, and it is more pronounced in the case of the 90/10 sample. After the 90/10 samples, the peaks are not shifting for other blend samples; however, it is observed that, in the blend samples, the intensity of PBI peaks are gradually decreasing and PVT peaks are gradually appearing with increasing PVT concentration. Figure 3 also shows that the PVT peaks are also shifting to the higher field. So this shifting in chemical-shift values indicates the presence of interactions between the two polymers. Thus, FT-IR and solid-state NMR studies agree well and prove the presence of an interaction between PBI and PVT.

**Absorption and Emission Spectroscopy.** The absorption and fluorescence emission spectra of PBI, PVT, and blend samples are studied in solid state. The absorption spectrum of PBI (Figure 4) in solid state shows two distinct peaks: a lower

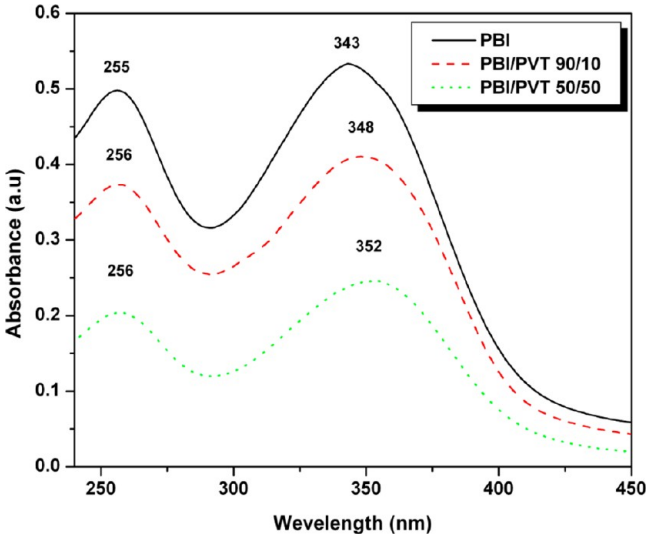


**Figure 4.** Absorption spectra of PBI and blend samples at the indicated composition. All the spectra were recorded in the solid state.

wavelength peak at ~255 nm and a higher wavelength absorption at ~343 nm.[45] The higher wavelength peak at 343 nm corresponds to the $\pi \rightarrow \pi^*$ transition. PVT does not display any absorption maxima. All the blend samples exhibit two distinct peaks. The intensity of these peaks is lower than that of PBI. This may because of a lower percentage of PBI in the blend. However, in the blends, the $\pi \rightarrow \pi^*$ peak is red-shifted significantly. This indicates more delocalized electron density in the imidazole moieties. The N–H groups of imidazole take part in the interaction with PVT in the case of blends, hence allowing more delocalization of electrons in the imidazole ring, resulting in a red-shift of the $\pi \rightarrow \pi^*$ peak.

The emission spectra of the PBI and blend samples recorded from solid state are shown in Figure 5. The emission spectrum

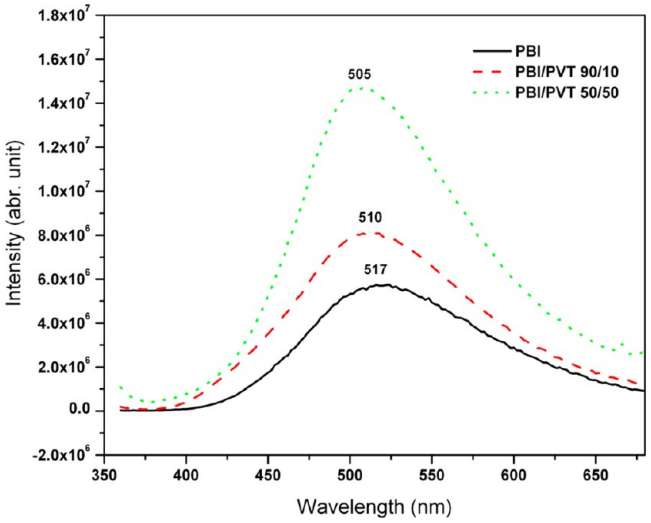


**Figure 5.** Fluorescence emission spectra of PBI and blend samples. The excitation wavelength ($\lambda_{exc}$) is 350 nm. All the spectra were recorded in the solid state.

of PBI shows one fluorescence band at 517 nm. Usually, PBI shows two emission bands, which are assigned to the 0–0 and 0–1 transitions from the excited $^1L_b$ state in the benzimidazole ring of PBI.[41,42,45] In this case, only one peak is observed, which is due to the 0–1 transition. The lower wavenumber is not observed in PBI, because, in the solid state, PBI is in the aggregated state.[41] The emission bands for blend samples are observed at lower wavelengths, relative to PBI. This blue-shifting of the emission bands in the blend samples can be attributed to the interactions between the polymers. The emission intensity of the blend samples increases as the PVT content in the blend increases (see Figure 5). This increase in intensity is quite unexpected, given the fact that, in the blend, the concentration of PBI is lower, compared to that of neat PBI. This unexpected intensity increase, in the case of the blend, may be due to increased electron delocalization that can be attributed to the strong interactions between the two polymers.

**Thermal Study.** The thermal stabilities of PBI, PVT, and blend membranes before and after doping with PA are performed under a nitrogen atmosphere at a heating rate of 10 °C/min. The representative TGA curves are shown in Figure 6. Two different weight losses are observed for PBI before doping (Figure 6A). The first weight loss, which occurs at ~100–120 °C, is due to loosely bound absorbed water molecules, and the second weight loss at 570–600 °C is because of the degradation of the polymer backbone. PVT shows an exponential weight decay up to 20% (by weight) until 300 °C, which can be attributed to absorbed water (Figure 6A). Above 350 °C, a remarkable weight loss is observed, which is due to the thermal decomposition of the side groups and the polymer chain. From Figure 6A, it is observed that all the blend samples in their undoped state are thermally stable up to 300 °C, except the initial weight loss, which varies, depending on the composition of the blend; this observation indicates that these are stable materials and can be used for high-temperature applications.

All the samples are doped with 85% PA for 3 days, and their TGA results show their first major weight loss between 50 °C and 150 °C, which corresponds to the water content of PA (Figure 6B) and loosely bound PA. After the initial weight loss,

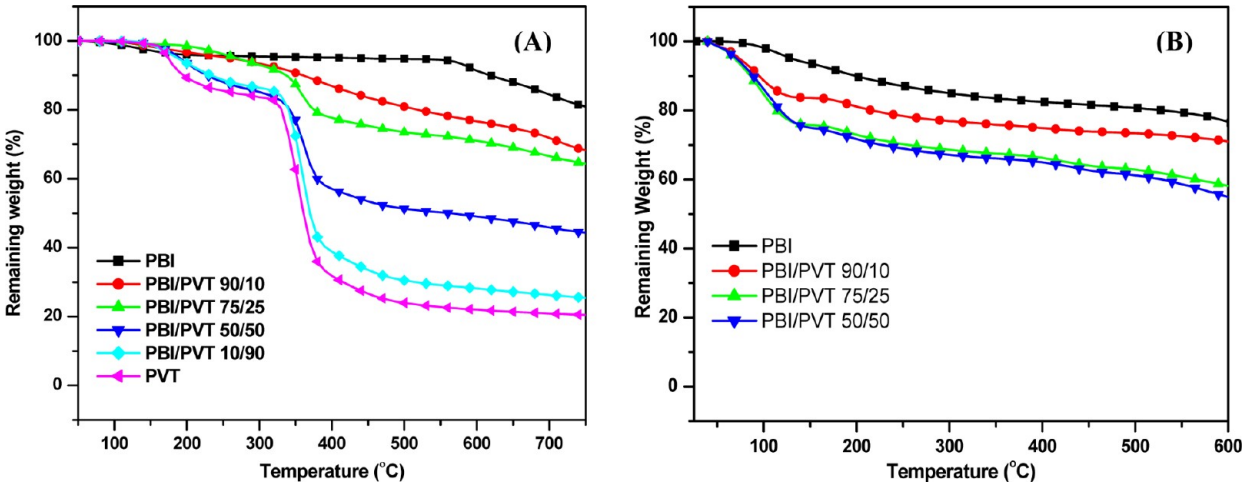


**Figure 6.** TGA curves of PBI, PVT, and blend samples (A) before doping and (B) after doping with PA at their indicated compositions.

a gradual weight loss is observed up to 600 °C, which is due to the successive dehydration of PA. The initial weight loss increases very nominally with increasing PVT content in the blend, because of the lower thermal stability of PVT.

**Miscibility Studies of Blends.** The films obtained after blending samples are homogeneous and transparent (see Figure 3 in the Supporting Information), indicating the miscibility of the two polymer components. The detailed FT-IR study and solid-state NMR study of these blend films evidenced the presence of specific interactions between the two polymers, which resulted in miscible blends. The miscibility of polymers blends can be easily determined by measuring the $T_g$ value of the blends. A miscible polymer blend exhibits only one $T_g$ value and when two polymers are partially miscible or completely immiscible, they exhibit more than one $T_g$ value, because they possess more than one phase and each phase undergoes its glass transition at a unique temperature corresponding to its composition.[46]

The glass-transition temperature ($T_g$) of the PBI, PVT, and blend samples are measured by using differential scanning calorimetry (DSC). The DSC measurement shows that the glass-transition temperatures of PBI and PVT are 362 and 153 °C, respectively. These $T_g$ values match well with the earlier reported values.[33−35,42] The DSC thermograms of PBI and blend samples are shown in Figure 7. It is observed that all the blends exhibit a single $T_g$ value, which decreases as the PVT content in the blend increases. This observation indicates the complete miscibility of the blends. The $T_g$ values of the blends are between the $T_g$ values of neat polymer, which also can be attributed to complete miscibility of the two polymers.

The Gordon−Taylor formula (eq 5) can be used to evaluate the dependency of $T_g$ on the blend composition.

$$T_g = \frac{W_1 T_{g1} + kW_2 T_{g2}}{W_1 + kW_2} \quad (5)$$

where $W$ is the weight fraction, $T_g$ is the glass-transition temperature of the blends, $T_{g1}$ and $T_{g2}$ are those of the pure components (PBI and PVT, respectively), and $k$ is an adjustable fitting parameter (the Gordon−Taylor constant) that describes the strength of the intermolecular interaction between the components in miscible polymer blends; the lower the value of $k$, the poorer the interaction.[47] The $T_g$ versus composition plot is shown in Figure 8. The dotted lines in Figure 8 are drawn using the Gordon−Taylor equation with $k$ values of 1 and 1.5. The $T_g$−composition curve of the PBI−PVT system forms a sigmoidal curve, as a function of composition, and it exhibits negative deviation from the Gordon−Taylor equation. The $T_g$ value fits well for $k$ = 1.5. It has been demonstrated in the literature that the resulting value of $k$ for thermodynamically miscible blends is close to unity, which is indicative of intimately mixed amorphous phases. Hence. our value of $k$, which is close to unity, proves that the present blend is a thermodynamically miscible blend. When the PVT concentration is low, the $T_g$ value of the blend is lower than the Gordon−Taylor $T_g$ value. However, at high PVT concentration (90%), the $T_g$ value is higher than the Gordon−Taylor $T_g$ value. Hence, the above fitting clearly indicates a strong intermolecular interaction between the polymers, which was also proved from spectroscopic studies, resulting in miscible blends.

**Morphological Study.** The blend membranes appear very homogeneous, which is attributed to miscibility (see Figure 3 in the Supporting Information). No phase separation is visible. This result is consistent with the FT-IR, SS-NMR, and DSC results. The homogeneity of the blend membranes are also studied by FE-SEM. The FE-SEM images of PBI, PVT, and a few representative blend images are shown in Figure 9. The morphology of PBI and PVT is featureless, which is consistent with earlier reports.[33−35,48] However, the morphology of the blend membranes is completely different from the neat polymers. It is interesting to note that blend samples exhibit a porous morphology and the pore size and nature are highly dependent on the blend composition. The porous morphology transforms to a particle morphology at high PVT contents of the blend. Figure 9 clearly demonstrates that the pore size increases with increasing PVT content in the blend; the bigger pores are seen in the case of the 75/25 blends; after that, pore size become smaller with increasing PVT content. Beyond 50/50 blends, the pores transform to particles, as seen in the case of the 10/90 samples. This morphology characteristic is seen throughout the membrane. We do not know the exact reason for this type of morphology; however, it can be said that, since the current blend is a miscible system, a new phase has been formed, which displays this type of morphology. Earlier, it was shown that the miscibility arises from the specific interactions, such as hydrogen bonding, or weak charge-transfer complexing can influence conformational changes of the individual polymer

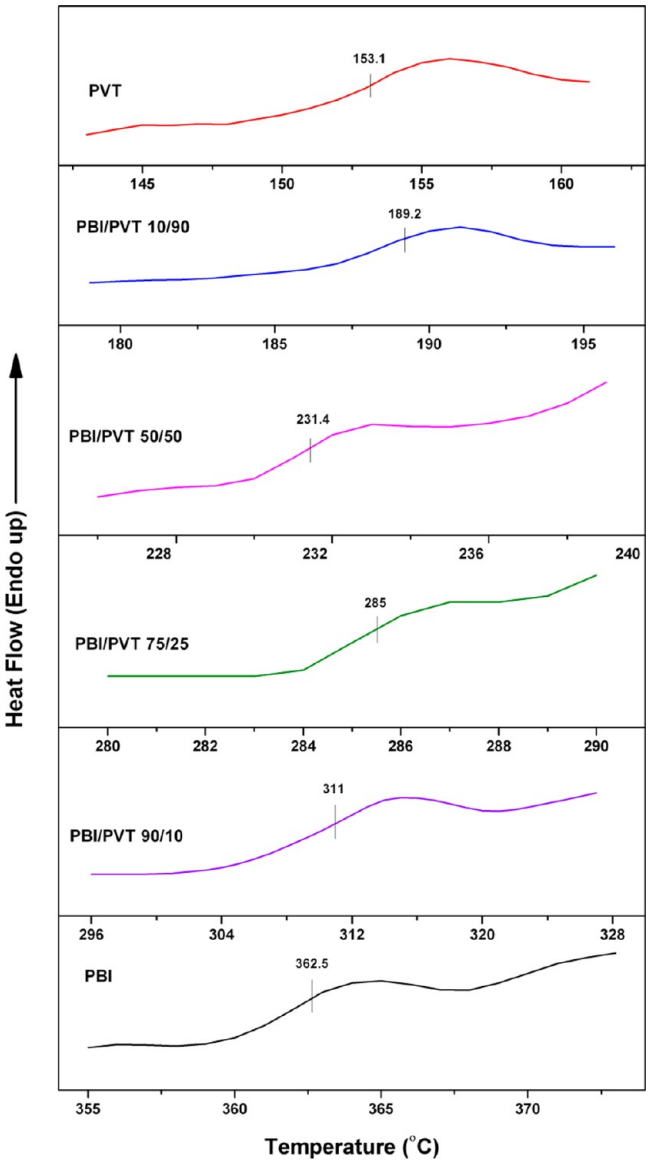


**Figure 7.** Differential scannign calorimetry (DSC) thermograms of neat PBI, PVT, and blends. The horizontal lines and the corresponding values in the thermograms are the $T_g$ values of the samples.

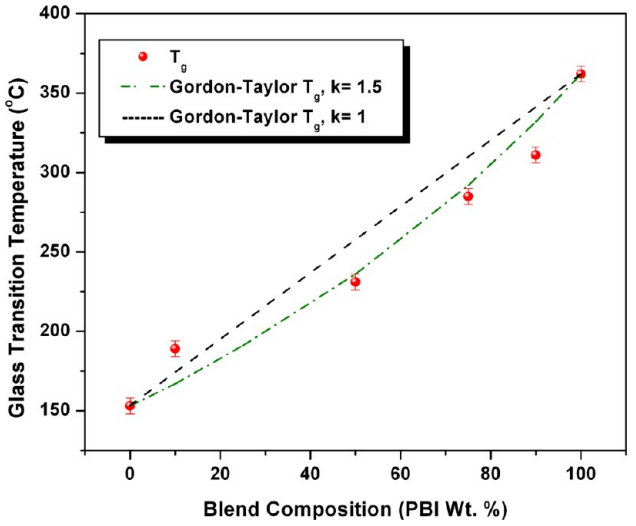


**Figure 8.** Variation of the glass-transition temperature ($T_g$) of the blend samples, as a function of blend composition. The solid red points are the experimentally obtained $T_g$ values from the DSC study, and the dotted lines are the calculated $T_g$ curve according to the Gordon–Taylor equation with $k$ = 1 and 1.5.

chains of the blends, which result in local ordering and microstructure in the miscible polymer blends.[49,50] We expect to see better properties of the blends compared to neat polymers which is the manifestation of this porous morphology. We have discussed the properties of the blends in the next few sections and it is indeed true that the blend properties are better than the neat polymers. The phosphoric acid doped PEMs are prepared by dipping these porous membranes in the PA bath, and it is reasonable to expect that the pores will be filled with PA and most likely with higher amount of PA. Recently significant number of reports in the literature also demonstrated that the microporous morphology can indeed be very useful to absorb the larger amount of PA.[51,52] Further work is in progress to study the suitability and durability of these membranes in a working PEMFC.

**Swelling Ratio and Thickness Increase in Phosphoric Acid.** The swelling ratio and thickness increase for the acid-doped membrane are important criteria of polyelectrolyte membrane for real fuel cell applications, because very thick membranes are not suitable for the membrane electrode assembly (MEA) fabrication. The PBI membrane increases in thickness quite significantly after PA doping. The swelling ratio, thickness increase, and PA loading of acid-doped PBI and blend membranes are shown in Table 1. From the table, it is observed that the swelling ratio and thickness increase of the blend membranes are significantly lower than those for PBI. Hence, these membranes are suitable for MEA fabrication. This significant decrease of swelling ratio and thickness in the case of blend membranes may be the result of their porous morphology. Because of these morphological features, when the blend membranes are dipped into PA, the porous structure of membrane accommodate the acid molecule in the pores, as a result of that, the thickness does not increase much, compared to that for neat PBI, and swelling of the membrane becomes less. The PA loading of the membrane increases with increasing PVT content in the blend (Table 1), since the N atoms of PVT can also interact and form acid–base complexes with the PA molecules. Also, the porous morphology of the blend membranes allows impregnation of a higher amount of PA.

**Proton Conductivity.** Proton conductivity of polyelectrolyte membrane is the most crucial property for a material to become a suitable PEM for use in fuel cells. The proton conductivities of all of the blend membranes are measured in the temperature range of 30–160 °C. All the membranes are immersed in PA solution for 3 days for acid doping before the measurement. The PA-loaded membranes are fixed in the homemade four-probe conductivity cell, and impedance is measured by varying the temperature from 30 °C to 160 °C. These first heating data are not reliable, because water is present in the membrane. Hence, after the first heating scan, we cooled the cell and again measured the impedance by varying the temperature. The conductivity data presented here represent the second heating data, and the conductivity is measured without any humidification. The proton conductivities of a few representative membranes obtained from the Nyquist plots (see Figure 4 in the Supporting Information) are plotted against temperature and shown in Figure 10. As

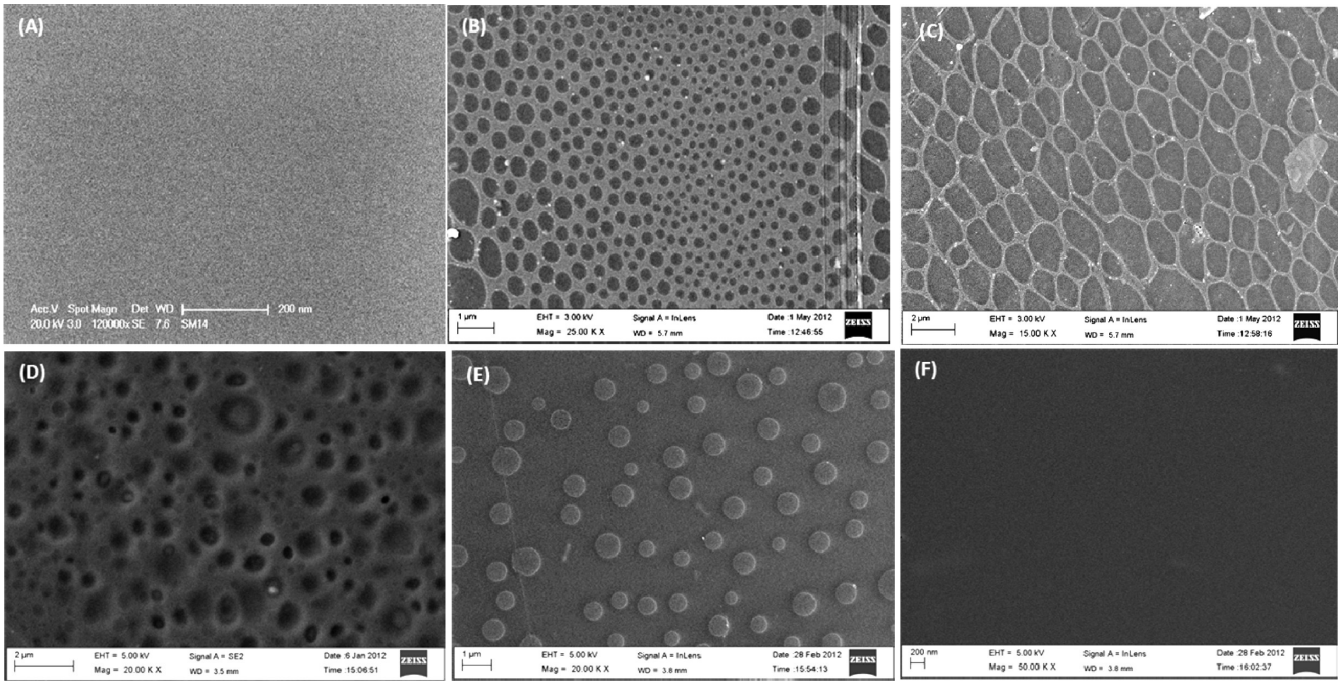


**Figure 9.** FE-SEM images of (A) PBI and PBI/PVT blends (B) 90/10, (C) 75/25, (D) 50/50, (E) 10/90, and (F) PVT.

**Table 1. Swelling and Acid Loading Data of Blend Membranes after Dipping in PA for 3 Days**[a]

| sample (PBI/PVT) | swelling ratio (%) | thickness increase (%) | PA loading (mol/PBI repeat unit) |
|---|---|---|---|
| 100/0 (PBI) | 43.13 (1.5) | 150 (23.54) | 10.21 (1.92) |
| 90/10 | 32.99 (0.16) | 41.66 (11.79) | 11.40 (0.46) |
| 75/25 | 39.03 (1.37) | 37.5 (0) | 15.85 (0.18) |
| 50/50 | 42.79 (1.2) | 49.93 (10) | 18.82 (2.31) |

[a]The standard deviations are shown in the parentheses.

expected in all of the cases, the proton conductivity increases with increasing temperature.

The proton conductivities of the blend samples are higher than that of the neat PBI. There are three reasons for the higher conductivity of blends: (i) because of the presence of both imidazole and triazole rings, the blend membranes are holding more PA, which increases the conductivity; (ii) because of the porous morphology; and (iii) because of the fact that triazole and imidazole rings are present in the same membrane and, hence, the proton conduction becomes more easy and feasible, compared to neat polymer. The proton conductivity of PBI at 160 °C is $3.9 \times 10^{-2}$ S/cm. For the 50/50 blend, the proton conductivity at 160 °C is $1.1 \times 10^{-1}$ S/cm, which is one order of magnitude higher, compared to neat PBI. Aslan et al. reported a maximum conductivity of PVT/(poly-(styrenesulfonic acid)$_2$ and PVT/(styrenesulfonic acid)$_4$ blend membrane is $1.5 \times 10^{-2}$ S/cm at 150 °C and under anhydrous conditions.[53] In another report, Günday et al. used 1H-1,2,4-triazole (Tri) as a proton solvent in different polymer host matrices, such as poly(vinylphosphonic acid) (PVPA), and poly(2-acrylamido-2-methyl-1-propane sulfonic acid) (PAMPS) to form PVPATri$_x$ and PAMPSTri$_x$, where $x$ is the molar ratio of Tri to the corresponding polymer repeat unit.[31] The maximum proton conductivity they could get is $2.3 \times 10^{-3}$ S/cm at 120 °C for PVPATri$_{1.5}$ and $9.3 \times 10^{-4}$ S/cm at 140 °C for PAMPSTri$_2$. In the literature, the reported conductivity of PVT at 150 °C is $5 \times 10^{-3}$ S/cm. However, when we tried to measure the conductivity of PA-doped PVT, it could not be measured after 60 °C. At high temperature (>60 °C), the dissolution of polymer in PA is observed, which is flowing out of the conductivity cell. We did not face any problem with our blend samples and could measure up to 160 °C. Therefore, the conductivity values for PBI/PVT blends are much higher than the reported values. Another reason for the high proton conductivity of the blend membranes is their morphology. The blend membranes have a porous morphology (Figure 9). Because of the presence of pores, the blend membranes can hold more PA than PBI. This increases the proton conductivity, since conductivity is directly proportional to the amount of PA in the membrane. Also, the porous nature of the membrane facilitates better proton conduction, resulting in high proton

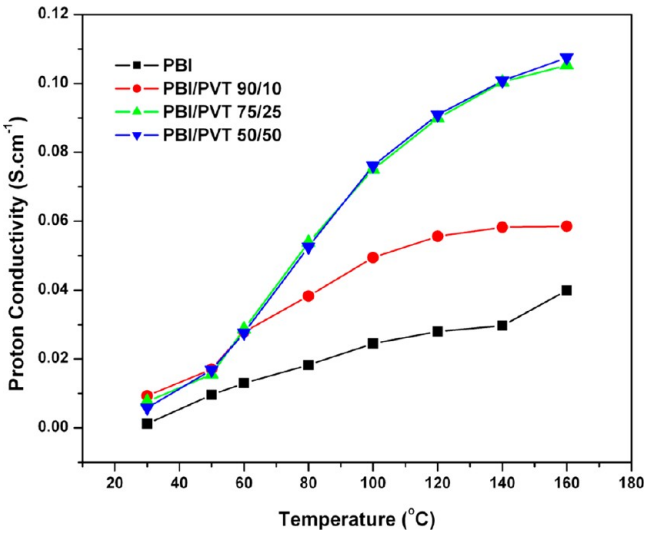


**Figure 10.** Proton conductivity versus temperature for PBI/PVT blend membranes.


dx.doi.org/10.1021/am301185b | ACS Appl. Mater. Interfaces 2012, 4, 5256−5265

conductivity. A careful comparison of morphology (Figure 9) and conductivity (Figure 10) data brings an important correlation between the morphology and conductivity of the membrane. The porous nature increases as we increase the PVT content (up to 75/25 composition); the conductivity also increases up to 75/25 and then slowly decreases, since the porous nature decreases after 75/25 composition. The 10/90 sample does not have a porous structure; hence, its conductivity is much lower, compared to other blends. Therefore, the morphology (microstructure) of the membrane influences the conductivity.

Two mechanisms contribute the proton transfer in PA-doped heterocyclic polymer electrolyte membranes. One is based on rapid proton exchange between phosphate and heterocyclic moieties via hydrogen bonds (the Grotthuss mechanism), and the second is based on the self-diffusion of phosphate moieties (the Vehicle mechanism).[54] For PA-doped membranes, the Grotthuss mechanism is the predominant mechanism for proton conduction.[55] To understand the conduction mechanism, the conductivity data is plotted against temperature, using the Arrhenius equation, as follows:

$$\ln(\sigma T) = \ln \sigma_0 - \frac{E_a}{RT} \quad (6)$$

where $\sigma$ is the protonic conductivity of the membrane (S $cm^{-1}$), $\sigma_0$ the pre-exponential factor (S $K^{-1}$ $cm^{-1}$), $E_a$ the proton-conducting activation energy (kJ $mol^{-1}$), $R$ the ideal gas constant (J $mol^{-1}$ $K^{-1}$), and $T$ the temperature (K). Arrhenius plots of the temperature-dependent conductivity are shown in Figure 11. The activation energy ($E_a$) is obtained from the slope of the linear fit of eq 6 and is shown in Figure 11. The data fit well with the equation, suggesting that the proton conduction is mainly governed by the Grotthuss mechanism. The $E_a$ values of the blend membranes are less, compared to that for PBI. This is because triazole and triazole derivatives act as proton transport facilitators for polymer electrolyte membranes.[33−35] That is why the proton conductivities of the blend membranes are higher than that of neat PBI. Also, a porous morphology facilitates faster proton conduction, resulting in lower $E_a$ value than that for neat PBI.

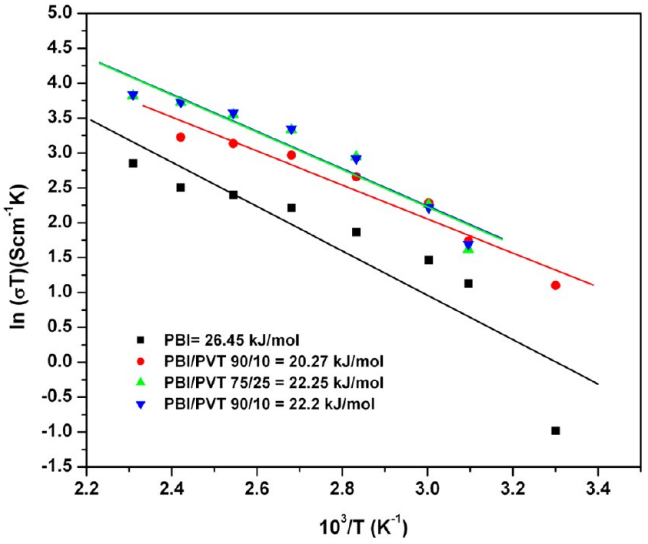


**Figure 11.** Arrhenius plots for the proton conduction of the blend samples at their indicated compositions.

## CONCLUSION

Novel blends of PVT and PBI of various compositions have been prepared using a solution blending technique. FT-IR and solid-state NMR, as well as photophysical studies, indicate the presence of a specific interaction between the two polymers, allowing them to form a miscible blend. The blend samples show a single composition-dependent $T_g$ value, which decreases as the PVT concentration in the blend increases. These observations suggest that PBI and PVT form a miscible blend. The N−H···N interaction between the two polymers is the driving force for this miscibility. The swelling ratio and thickness increase of the blend samples are smaller than those of PBI. The proton conductivity of the blend membranes is higher than that of the neat PBI and increases as the PVT concentration increases, up to the 75/25 (PBI/PVT) composition. The morphology of the blends governs the conduction behavior of the blends. These thermomechanically stable, highly conducting blends may be suitable for use as proton exchange membranes (PEMs) in high-temperature fuel cells.

## ASSOCIATED CONTENT

### Supporting Information

Figures showing FT-IR and solid-state NMR spectra of PVT, photographs of the blend samples, and Nyquist plots of PBI and blend membranes. This information is available free of charge via the Internet at http://pubs.acs.org/.

## AUTHOR INFORMATION

### Corresponding Author

*Tel.: (91) 40 23134808. Fax: (91) 40 23012460. E-mail: tjsc@uohyd.ernet.in tjscuoh@gmail.com.

### Notes

The authors declare no competing financial interest.

## ACKNOWLEDGMENTS

We gratefully acknowledge the financial support by DST (Grant No. SR/SI/PC58/2008). M. H. thanks CSIR for the senior research fellowship. We sincerely thank S. Srinath of School of Physics, University of Hyderabad for his help with FE-SEM study. We also thank Mr. S. Maity for his generous help with acid loading measurements during the revision of this manuscript.

## REFERENCES

(1) Blomen, L. J. M. J.; Mugerwa, M. N. In *Fuel Cell Systems*; Plenum Press: New York, 1993.
(2) Peighambardoust, S. J.; Rowshanzamir, S.; Amjadi, M. *Int. J. Hydrogen Energy* **2010**, *35*, 9349−9384.
(3) Trogadas, P.; Ramani, V. In *Encyclopedia of Electrochemical Power Sources*; Academic Press: Amsterdam, 2009; pp 716−723.
(4) Rikukawa, M.; Sanui, K. *Prog. Polym. Sci.* **2000**, *25*, 1463−1502.
(5) Kerres, J. A. *J. Membr. Sci.* **2001**, *185*, 3−27.
(6) Asensio, J. A.; Sánchez, E. M.; Gómez-Romero, P. *Chem. Soc. Rev.* **2010**, *39*, 3210−3239.
(7) Zhang, H.; Shen, P. K. *Chem. Rev.* **2012**, *112*, 2780−2832.
(8) Li, Q.; He, R.; Jensen, J. Q.; Bjerrum, N. J. *Chem. Mater.* **2003**, *15*, 4896−4925.
(9) Seel, D. C.; Benicewicz, B. C. *J. Membr. Sci.* **2012**, *405*, 57−67.
(10) Mader, J. A.; Benicewicz, B. C. *Macromolecules* **2010**, *43*, 6706−6715.
(11) Bose, S.; Kuila, T.; Nguyen, T. X. H.; Kim, N. H.; Lau, K.-t.; Lee, J. H. *Prog. Polym. Sci.* **2011**, *36*, 813−843.

(12) Parka, C. H.; Leeb, C. H.; Guivera, M. D.; Lee, Y. M. *Prog. Polym. Sci.* **2011**, *36*, 1443−1498.
(13) Li, Q.; Jensena, J. O.; Savinell, R. F.; Bjerrum, N. J. *Prog. Polym. Sci.* **2009**, *34*, 449−447.
(14) Shao, V.; Yin, G.; Wang, Z.; Gao, Y. *J. Power Sources* **2007**, *167*, 235−242.
(15) Scharfenberger, G.; Meyer, W. H.; Wegner, G.; Schuster, M.; Kreuer, K. D.; Maier, J. *Fuel Cells* **2006**, *6* (3−4), 237−250.
(16) Granados-Focil, S.; Woudenberg, R. C.; Yavuzcetin, O.; Tuominen, M. T.; Coughlin, E. B. *Macromolecules* **2007**, *40*, 8708−8713.
(17) Nagamani, C.; Versek, C.; Thorn, M.; Tuominen, M. T.; Thayumanavan, S. *J. Polym. Sci., Polym. Chem.* **2010**, *48*, 1851−1858.
(18) Michael, A. H.; Hossein, G.; Yu, S. K.; Brian, R. E.; James, E. M. *Chem. Rev.* **2004**, *104*, 4587−4612.
(19) Zhou, Z.; Li, S.; Zhang, Y.; Liu, M.; Li, W. *J. Am. Chem. Soc.* **2005**, *127*, 10824−10825.
(20) Kreuer, K. D.; Fuchs, A.; Ise, M.; Spaeth, M.; Maier, J. *Electrochim. Acta* **1998**, *43*, 1281−1288.
(21) Schuster, M. F. H.; Meyer, W. H.; Schuster, M.; Kreuer, K. D. *Chem. Mater.* **2004**, *16*, 329−337.
(22) Li, S.; Zhou, Z.; Zhang, Y.; Liu, M.; Li, W. *Chem. Mater.* **2005**, *17*, 5884−5886.
(23) Martwiset, S.; Woudenberg, R. C.; Granados-Focil, S.; Yavuzcetin, O.; Tuominen, M. T.; Coughlin, E. B. *Solid State Ionics* **2009**, *178*, 1398−1403.
(24) Sanghi, S.; Tuominen, M.; Coughlin, E. B. *Solid State Ionics* **2010**, *181*, 1183−1188.
(25) Subbaraman, R.; Ghassemi, H.; Zawodzinski, T. A., Jr. *J. Am. Chem. Soc.* **2007**, *129*, 2238−2239.
(26) Subbaraman, R.; Ghassemi, H.; Zawodzinski, T., Jr. *Solid State Ionics* **2009**, *180*, 1143−1150.
(27) Maalouf, M.; Ghassemi, H.; Zawodzinski, T. A. *ECS Trans.* **2010**, *25*, 19−25.
(28) Saito, J.; Miyatake, K.; Watanabe, M. *Macromolecules* **2008**, *41*, 2415−2420.
(29) Aslan, A.; Bozkurt, A. *J. Power Sources* **2009**, *191*, 442−447.
(30) Çelik, S. Ü.; Akbey, Ü.; Bozkurt, A. *Macromol. Chem. Phys.* **2008**, *209*, 593−603.
(31) Günday, S. T.; Bozkurt, A.; Meyer, W. H.; Wegner, G. *J. Polym. Sci., Part B: Polym. Phys.* **2006**, *44*, 3315−3322.
(32) Ozden, S.; Celik, S. U.; Bozkurt, A. *J. Polym. Sci., Polym. Chem.* **2010**, *48*, 4974−4980.
(33) Çelik, S. Ü.; Aslan, A.; Bozkurt, A. *Solid State Ionics* **2008**, *179*, 683−688.
(34) Aslan, A.; Celik, S. U.; Sen, U.; Haser, R.; Bozkurt, A. *Electrochim. Acta* **2009**, *54*, 2957−2961.
(35) Celik, S. U.; Sen, U.; Haser, R.; Bozkurt, A. *J. Polym. Sci., Polym. Phys.* **2010**, *48*, 1016−1021.
(36) Sen, U.; Bozkurt, A.; Ataa, A. *J. Power Sources* **2010**, *195*, 7720−7726.
(37) Musto, P.; Karasz, F. E.; MacKnight, W. J. *Macromolecules* **1991**, *24*, 4762−4769.
(38) Deimede, V.; Voyiatzis, G. A.; Kallitsis, J. K.; Qingfeng, L. N.; Bjerrum, J. *Macromolecules* **2000**, *33*, 7609−7617.
(39) Arunbabu, D.; Sannigrahi, A.; Jana, T. *J. Phys. Chem. B* **2008**, *112*, 5305−5310.
(40) Hazarika, M.; Arunbabu, D.; Jana, T. *J. Colloid Interface Sci.* **2010**, *351*, 374−383.
(41) Sannigrahi, A.; Arunbabu, D.; Sankar, R. M.; Jana, T. *Macromolecules* **2007**, *40*, 2844−2851.
(42) Sannigrahi, A.; Arunbabu, D.; Sankar, R. M.; Jana, T. *J. Phys. Chem. B* **2007**, *111*, 12124−12132.
(43) Xue, H.; Gao, H.; Shreeve, J. M. *J. Polym. Sci., Part A: Polym. Chem.* **2008**, *46*, 2414−2421.
(44) Grobelny, J.; Rice, D. M.; Karasz, F. E.; MacKnight, W. J. *Macromolecules* **1990**, *23*, 2132−2139.
(45) Sannigrahi, A.; Ghosh, S.; Lalnuntluanga, J.; Jana, T. *J. Appl. Polym. Sci.* **2009**, *111*, 2194−2203.
(46) Cakar, F.; Sakar, D.; Cankurtaran, O.; Karaman, F. *Eur. Polym. J.* **2007**, *43*, 507−513.
(47) Ahn, T.-K.; Kim, M.; Choe, S. *Macromolecules* **1997**, *30*, 3369−3374.
(48) Sannigrahi, A.; Ghosh, S.; Maity, S.; Jana, T. *Polymer* **2011**, *11*, 4319−4330.
(49) Utracki, L. A. In *Polymer Blends Handbook*; Kluwer Academic Publishers: Dordrecht, The Netherlands, 2002.
(50) Saito, H.; Takahashi, M.; Inoue, T. *Macromolecules* **1991**, *24*, 6356−6358.
(51) Mecerreyes, D.; Grande, H.; Miguel, O.; Ochoteco, E.; Marcilla, R.; Cantero, I. *Chem. Mater.* **2004**, *16*, 604−607.
(52) Shen, C.-H.; Jheng, L.-C; Hsu, S. L.-C.; Wang, J. T.-W. *J. Mater. Chem.* **2011**, *21*, 15660−15665.
(53) Aslan, A.; Sen, U.; Bozkurt, A. *J. Electrochem. Soc.* **2009**, *156*, B1112−B116.
(54) Pu, H.; Meyer, W. H.; Wegmer, G. *J. Polym. Sci., Part B: Polym. Phys.* **2002**, *40*, 663−669.
(55) Yu, S.; Benicewicz, B. C. *Macromolecules* **2009**, *42*, 8640−8648.